Commun. Theor. Phys. **75** (2023) 045503 (8pp) https://doi.org/10.1088/1572-9494/acbe2d

Active tunable terahertz bandwidth absorber based on single layer graphene

Wenxin Li[1,6], Yingting Yi[2,6], Hua Yang[3], Shubo Cheng[1,*], Wenxing Yang[1,*], Huafeng Zhang[1], Zao Yi[1,4,*], Yougen Yi[2] and Hailiang Li[5]

[1] School of Physics and Optoelectronic Engineering, Yangtze University, Jingzhou 434023, China
[2] College of Physics and Electronics, Central South University, Changsha 410083, China
[3] School of Science, Lanzhou University of Technology, Lanzhou 730050, China
[4] Joint Laboratory for Extreme Conditions Matter Properties, Southwest University of Science and Technology, Mianyang 621010, China
[5] Key Laboratory of Microelectronic Devices & Integrated Technology, Institute of Microelectronics, Chinese Academy of Sciences, Beijing 100029, China

E-mail: shubocheng@yangtzeu.edu.cn, wenxingyang2@126.com and yizaomy@swust.edu.cn

Received 23 November 2022, revised 22 February 2023
Accepted for publication 23 February 2023
Published 17 April 2023

Abstract

In this paper, an active tunable terahertz bandwidth absorber based on single-layer graphene is proposed, which consists of a graphene layer, a photo crystal plate, and a gold substrate. When the Fermi energy (E_f) of graphene is 1.5 eV, the absorber shows high absorption in the range of 3.7 THz–8 THz, and the total absorption rate is 96.8%. By exploring the absorption mechanism of the absorber, the absorber shows excellent physical regulation. The absorber also shows good adjustability by changing the E_f of graphene. This means that the absorber exhibits excellent tunability by adjusting the physical parameters and E_f of the absorber. Meanwhile, the absorber is polarization independent and insensitive to the incident angle. The fine characteristics of the absorber mean that the absorber has superior application value in many fields such as biotechnology and space exploration.

Keywords: metamaterials, active tunable, bandwidth absorber, terahertz, graphene

(Some figures may appear in colour only in the online journal)

1. Introduction

The terahertz wave range is 3000–30 μm [1–3]. Its electromagnetic wave is consistent with the infrared light in the shortwave band and the millimeter wave in the longwave band [4, 5]. It covers macro theory, micro quantum, and other disciplines [6, 7]. Since the terahertz band includes characteristic spectra of semiconductors, plasma, biology, and biological macromolecules, terahertz has high application value in the fields of material science, military science and technology, information and communication technology, confidential communication, and medical technology [8–11]. The terahertz band is very important in astrophysics because terahertz radiation contains most of the luminosity of the Universe and 98% of the photons generated by the Big Bang are in the THz frequency domain.

Tunable metamaterials are an important component of various optical devices but these materials are extremely rare in the terahertz frequency range [12–16]. After Tao *et al* designed the first THz absorber based on metamaterials in 2008 [17], metamaterial-based absorbers have attracted extensive research and attention [18–22]. In 2014, Wang *et al* designed a bandwidth absorber in the THz band through alloy metamaterials. The absorber has two perfect absorption peaks, which can reach an absorption rate of more than 0.9 in the range of about 3 THz and can be tuned by the physical parameters of the absorber [23]. In 2015, Wen *et al* designed a bandwidth absorber using gold and the absorption rate of the absorber was higher than 0.9 in the 4.4 THz–5.2 THz [24]. In 2016, Guo *et al* designed an infrared band absorber using metal. Its absorption rate in the 7.9 THz–12 THz is

[6] These authors contributed equally to this work and should be considered co-first authors.
[*] Authors to whom any correspondence should be addressed.

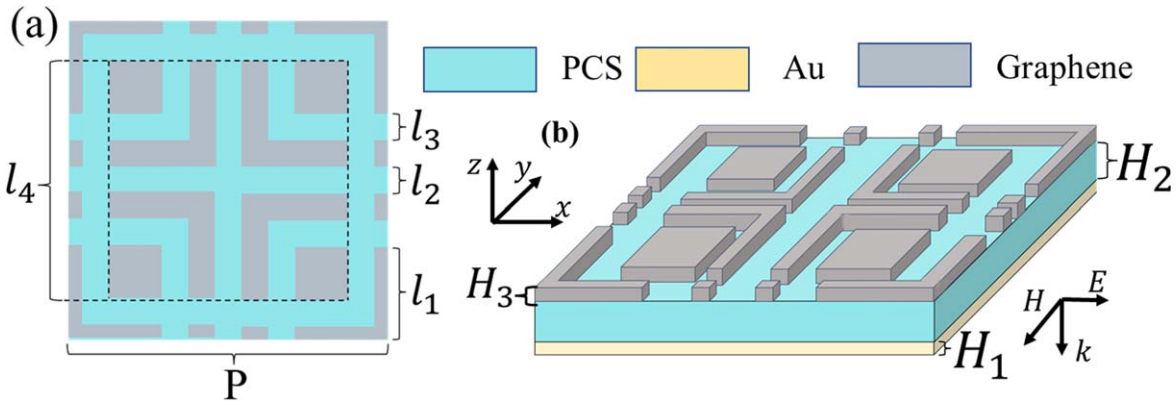

Figure 1. (a) The plane of the absorber and (b) a structural drawing of the absorber.

higher than 0.9, and the characteristics of the absorber can be tuned through physical parameters [25]. As a tunable metamaterial with good response in the terahertz range, graphene has been extensively studied as an absorbent [26–30]. It can dynamically adjust E_f by applying a bias voltage to change its electrical characteristics [31–34]. In 2016, Wang *et al* used multilayer graphene to design a bandwidth absorber that can be in the range of 3–3.8 Thz and can tune the characteristics of the absorber through physical parameters and E_f [15]. In 2018, Yang *et al* used a dielectric material and graphene to design a bandwidth absorber with an absorption rate higher than 0.9 in the 1.6 THz–3.1 THz [16]. In 2018, Liu *et al* designed a tunable THz absorber using single-layer graphene, and its absorption at 7–9.25 THz was higher than 0.9 [35]. It can be seen that the THz bandwidth absorber based on single-layer graphene still has great research value.

In this paper, an active tunable terahertz bandwidth absorber based on single-layer graphene is proposed. When the E_f is 1.5 eV, the absorber consists of a layer of graphene and a layer of optical crystal plate, and the substrate is gold. The absorber continuously absorbs electromagnetic waves with high absorption (higher than 0.9) rate in the range of 4.3 THz. The overall absorption rate of the absorber is 96.8% at 3.7–8 THz and there are perfect absorption peaks at 4.1 THz and 6.7 THz. By setting two different modes (TE and TM), the absorber shows good polarization incoherence. The change of relative impedance Z in the absorption frequency band is analyzed. Then, by observing the electric field of 4.1 THz and 6.7 THz, the relationship between the absorption mechanism of the absorber and the geometric parameters is analyzed. The absorber can also tune the absorption characteristics of the absorber by changing the E_f of graphene. Especially, when the E_f of graphene is 2, the high absorption region of the absorber was up to 4.6 THz. Also, fine absorption stability can be maintained under different electromagnetic wave incidence angles. The excellent characteristics of the absorber mean that it has high application value in many fields.

2. Structure design and unit cell model

In this paper, the proposed absorber unit cell consists of three layers, with graphene on the top layer and gold on the substrate separated by a layer of photonic crystal slab (PCS). Figure 1 shows the top view (figure 1(a)) and a structural drawing of the absorber (figure 1(b)). Through simulation analysis and the optimization of CST Microwave Studio, the proposed efficient broadband absorber is simulated and the periodic boundary conditions are applied to the simulation of infinite periodic elements [36–38]. Through careful optimization, the parameters of the absorber are obtained. The P is 60 μm. l_1, l_2, l_3 and l_4 are 10 μm, 3.16 μm, 5 μm and 45 μm respectively. The top of the absorber is graphene and its thickness is 1 nm, the PCS below is 11 μm, and the gold is 300 nm.

The conductivity of graphene can be derived from the famous Kubo formula, and its final result is as follows [39]:

$$\sigma(\omega) = \frac{e^2 E_f}{\pi\hbar^2}\frac{i}{\omega + i\tau^{-1}}, \tag{1}$$

where the $\tau = \mu E_f / e v_f{}^2$ is carrier relaxation lifetime and the carrier density μ is 10, 000 $cm^2\ V^{-1}s^{-1}$.

The Fermi velocity is $v_f = c/300$ and the dielectric constant of graphene can be confirmed by [40]:

$$\varepsilon = 1 + \frac{i\sigma(\omega)}{\varepsilon_0 t\omega}, \tag{2}$$

where t is the thickness of the graphene, and ε_0 is the permittivity of the vacuum. The dielectric constant of the PCS is 1.56.

3. Results and discussion

S_{11} is obtained through CST simulation calculation. Then the absorption rate is defined as $A = 1-|S_{11}|^2$. Figure 2(a) is the absorption spectrum of the different polarization electromagnetic wave incidence. It is obvious that the absorber has strong absorption (greater than 0.9) at 3.7–8 THz and the total absorption rate is 96.8%. The absorption spectra show perfect absorption peaks at $\lambda_1 = 4.1$ THz and $\lambda_2 = 6.7$ THz. From the absorption spectra in both

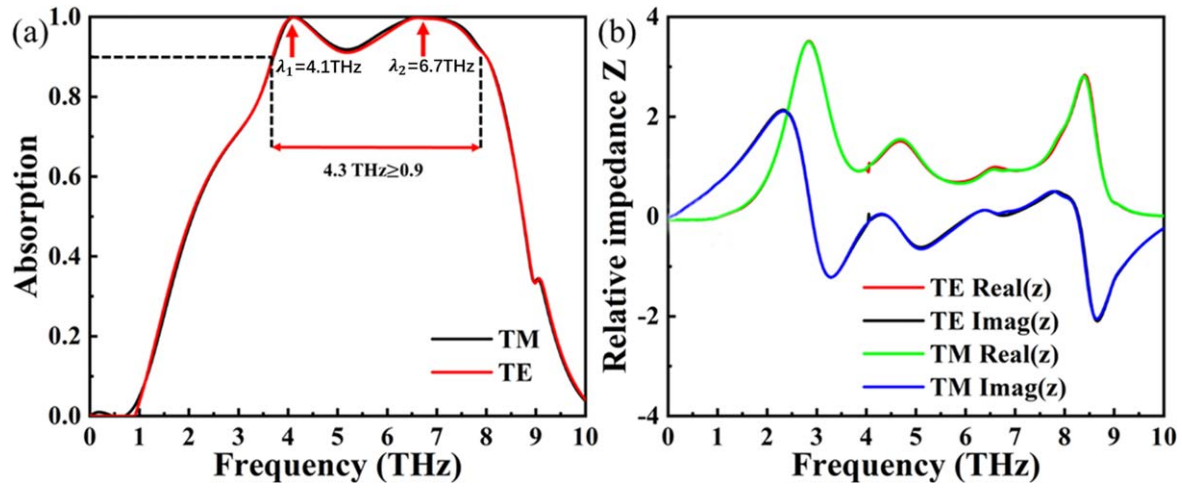

Figure 2. (a) Absorption spectra in two polarization modes (TM and TE) (b) Relative impedance under two polarization modes (TM and TE).

polarization modes (the polarization direction of TE is the x-axis and the polarization direction of TM is the y-axis), it is obvious that the absorber exhibits excellent polarization incoherence. Due to the symmetry of the structure, when the electromagnetic waves with different polarization modes are absorbed, the electric dipole will produce similar vibration, which is shown as polarization incoherence on the macro level. Generally speaking, the absorber shows high absorption characteristics when the relative impedance of the absorber is the same as the impedance in the space. The relative impedance Z of the absorber can be determined by [41, 42]:

$$Z = \pm\sqrt{\frac{1 + {S_{11}}^2 - S_{21}^2}{1 - {S_{11}}^2 - S_{21}^2}}. \tag{3}$$

Figure 2(b) shows the relative impedance of the absorber under the two polarization modes. It is obvious that when the absorber shows high absorption (3.7 THz–8 THz), the relative impedance of the absorber is drawn near space impedance, and when the absorption of the absorber is not high, the relative impedance is far away from the space impedance. At the same time, the relative impedance of the two modes is almost the same, which more intuitively reflects the polarization incoherence of the absorber.

Figure 3 shows the electric field diagram and a locally enlarged diagram of the absorber under the two modes. For the convenience of discussion, the absorber is divided into four areas and the local magnified view of the absorber comes from these areas. For the convenience of discussion, the absorber is divided into four zones, zones 1, 2, 3 and 4 (figure 3(a)). The local magnified view of the absorber comes from these areas. Figure 3(b) shows that when the TE wave is at $\lambda_1 = 4.1$ THz, the absorber mainly passes through the strong electric field coupling effect of zones 2, 3 and 4, which is due to the electric dipole resonance caused by the horizontal electric field [43–45]. The resonance coupling mainly depends on the properties, shape and scale of the material. This response of the absorber means that the structure proposed in this paper is reasonable and effective. According to figure 3(c), we can see that when the TE wave is $\lambda_2 = 6.7$ THz, the absorber has the strong electric field coupling effect of zones 1, 2 and 3, and the strong vibration generated by the electric dipole makes the electromagnetic wave lose a lot of energy, thus showing a very high electromagnetic wave absorption rate.

Figure 3(d) shows that when the TM wave is $\lambda_1 = 4.1$ THz, the absorber mainly passes through the strong electric field coupling effect of Zone 1, Zone 3 and Zone 4. Similarly, according to figure 3(e), when the TM wave is $\lambda_2 = 6.7$ THz, the absorber mainly passes through the strong electric field coupling effect of Zone 1, 2, 3 and 4. According to the vibration position of each Zone, we can infer that the absorption characteristics of the absorber may be related to the geometric parameters. This means that the absorption characteristics of the absorber can be changed by adjusting the geometric parameters.

In order to demonstrate the conjecture, we observe the change in the absorption spectrum of the absorber by changing different physical parameters. In figure 4(a), by changing the performance of the P-tuned absorber, we can see that when P rises from 44 μm to 76 μm, the absorption spectrum undergoes a redshift. The perfect absorption peak is around 4.6 THz when the P is 44 μm. The perfect absorption peak is around 4.4 THz when the P is 52 μm. The perfect absorption peak is around 3.9 THz and 6.3 THz when the P is 68 μm. As the absorber performance declines, there are absorption peaks around 3.8 and 6.8 THz when the P is 76 μm.

From figure 4(b), it is obvious that the absorption spectrum of the absorber shows a red shift as H_2 increases from 9 μm to 13 μm. When H_2 is 9 μm, the absorption efficiency of the absorber is not significant, and the absorption peaks appear at 4 THz and 6.5 THz. When H_2 is 10 μm, the absorption peak of the absorber also appears at 4 THz and 6.5 THz, and the absorption efficiency is further improved. When H_2 is 12 μm, the perfect absorption peak is at 4 THz and 6.8 THz. The high absorption position of the absorption spectrum at this time is higher than that at $H_2 = 11$, but the absorption range at this time is only 3.9 THz (3.5–7.4 THz).

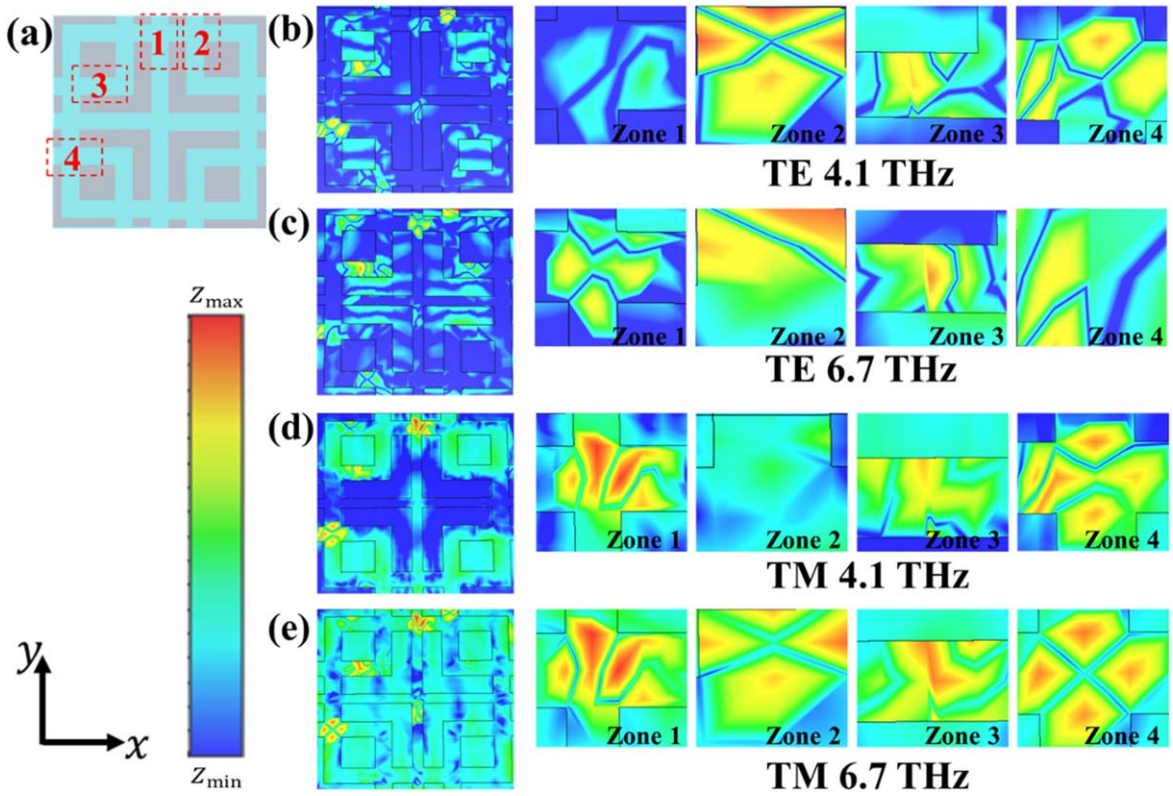

Figure 3. (a) Absorber area division diagram (b) Electric field of TE wave at 4.1 THz (c) Electric field of TE wave at 6.7 THz (d) Electric field of TM wave at 4.1 THz (e) Electric field of TM wave at 6.7 THz.

When H_2 is 13 μm, the perfect absorption peak is at 4 THz and 5.5 THz, and the strong absorption range is only 3.5 THz (3.5 THz–7 THz). It can be seen that with the increase of H_2, the strong absorption of the absorption spectrum will be enhanced but the strong absorption range will be reduced, so the appropriate H_2 can be selected according to the needs.

Figure 4(c) shows the absorption spectra of the absorber at different l_2. It is obvious that the absorption spectra show a slight blue shift with the increase of l_2. The variation range of l_2 in the figure is 2.26 μm–5.22 μm. It can be found that the absorption peak near 4.1 THz will not be affected by the variation of l_2, but with the gradual increase of l_2, the perfect absorption peak near 6.7 THz gradually weakens and has a significant blue shift, which ultimately leads to the absorption rate of the absorber for electromagnetic waves near 6.7 THz dropping to around 0.9. As can be seen from figure 3, when l_2 is changed, the affected location is mainly zone 1. By comparing figures 4(b) and (c), it can be inferred the reason for this phenomenon is that the absorber absorbs TE waves at 6.7 THz, part of which comes from the strong electromagnetic coupling effect in Zone 1, while changing l_2 has an impact on the strong electromagnetic coupling effect there, thus causing the absorber to reduce its absorption of TE wave at 6.7 THz.

Figure 4(d) shows the absorption spectra at different the l_4. It is obvious from the figure that as the l_4 increases from 39 μm to 51 μm, the absorption spectra will have a redshift. When the l_4 is 39 μm, there are absorption peaks near 5.2 THz and 7 THz in the absorption spectrum, where 5.2 THz is the perfect absorption peak and the high absorption part is about 3 THz (4.5–7.5 THz). When the l_4 is 42 μm, the absorption spectrum has a perfect absorption peak near 4.6 THz and 6.7 THz and the high absorption part is about 3.7 THz (3.9–7.6 THz). When the l_4 is 48 μm, the absorption spectrum has perfect absorption peaks around 3.8 THz and 6.7 THz. Meanwhile, the high absorption part of the absorber is 3.6 THZ–8 THz, but the absorption rate of about 1 THz is lower than 0.9 (4.5–5.5 THz). When the l_4 is 51 μm, the absorption spectrum has a perfect absorption peak near 3.4 THz and 6.7 THz. Meanwhile, the high absorption part of the absorber has 3.5 THz (3–3.8 THz, 4.5–4.8 THz, and 5.7–8.1 THz). It is obvious that with the increase of the l_4, the absorption peak near 6.7 THz basically remains unchanged, while the redshift of the other absorption peak is more obvious. It is obvious from figure 3(a) that when l_4 is changed, zone 1 and zone 4 will be affected. By comparing figure 3(a) and figure 3(b), it can be inferred that this phenomenon is due to the absorption of 4.1 THz partly due to the strong electric field coupling effect in zone 4 [46]. Changing the l_4 will affect it, thus the absorption peak changed. It can be considered that in the above results, we change the strength and position of the dipole resonance in some zones by changing the physical parameters so that the whole absorber shows different characteristics.

In general, by changing the physical parameters of the absorber such as the absorption position and absorption width, other indicators of the absorber can be effectively tuned, which indicates that the absorber has a strong physical tuning ability.

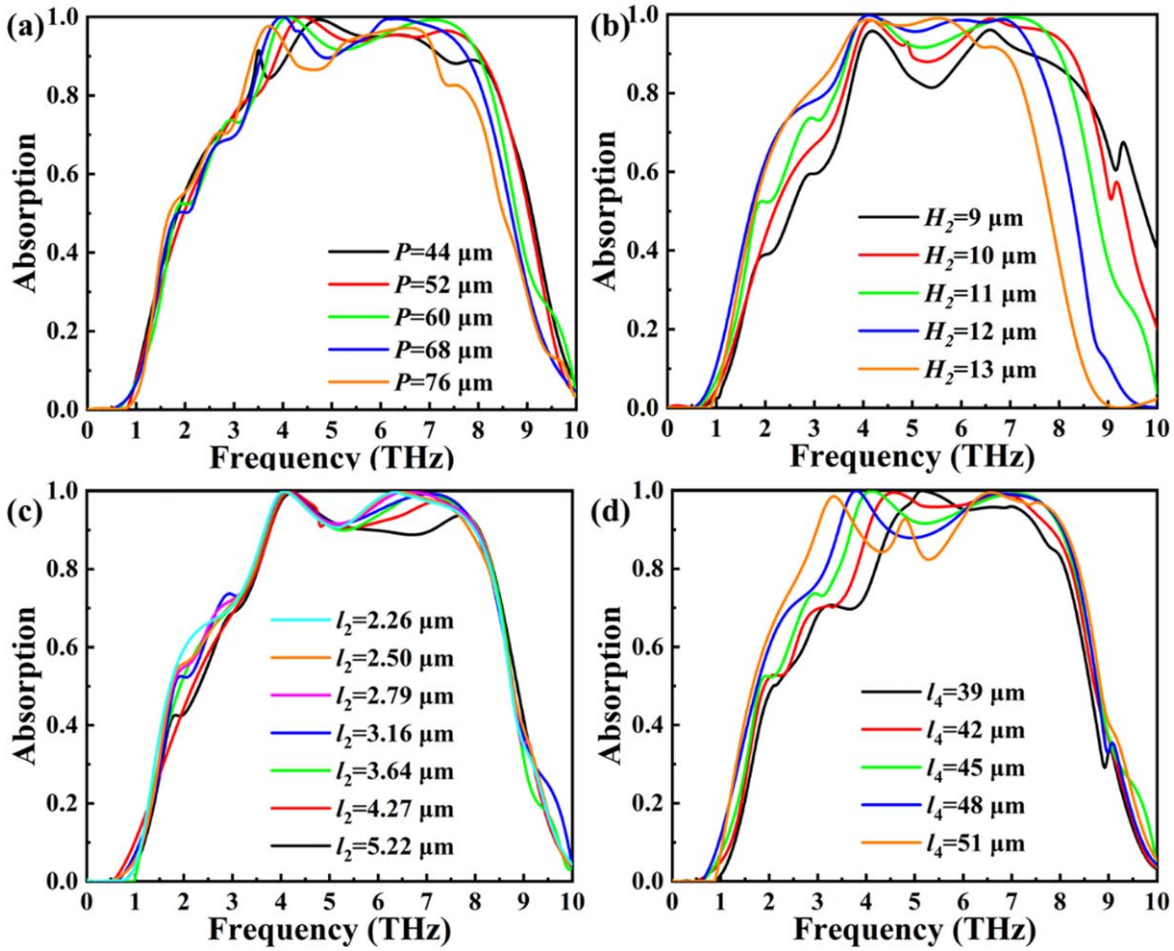

Figure 4. Influence of geometrical parameters on absorber characteristics. (a) Absorber characteristics change with P, (b) absorber characteristics change with H_2, (c) and absorber characteristics change with l_2. (d) Absorber characteristics change with l_4.

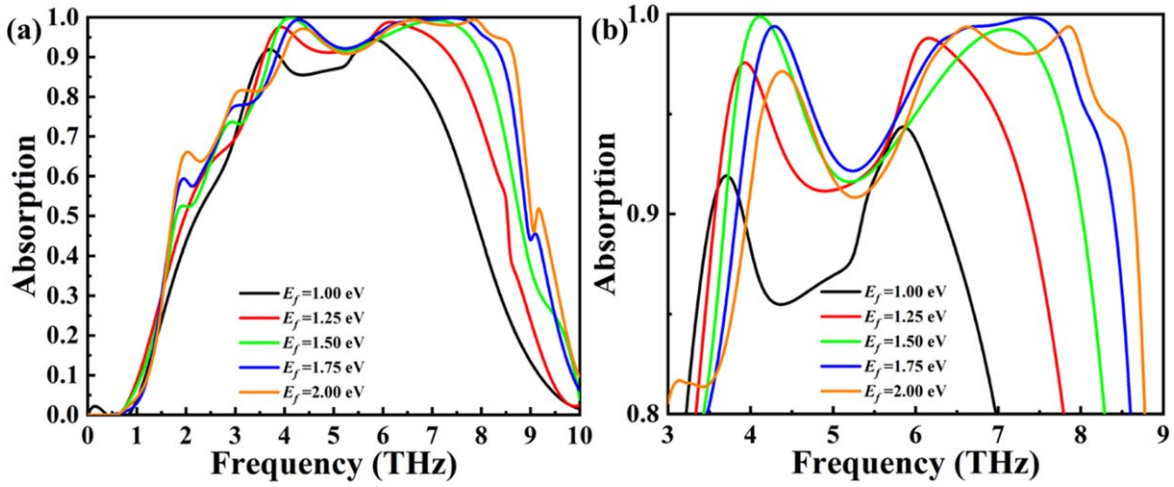

Figure 5. (a) Absorber characteristics E_f.(b) Partially enlarged view of (a).

Due to the excellent E_f tuning property of graphene, this paper has deeply studied the influence of graphene E_f change on the absorption spectrum, as shown in figure 5. It is obvious that when E_f is increased from 1 eV to 2 eV, the absorption spectrum is blueshifted and the position of the absorption peak changes (figure 5(a)). Figure 5(b) is a partially enlarged view of figure 5(a). It is obvious that when E_f is 1 meV, the absorption peaks of the absorber appear at 3.7 THz and 5.8 THz. At this time, only the absorption of 1.4 THz is higher than 0.9 (3.5–3.8 THz). When E_f is 1.25 eV, the absorption peak of the absorber appears at 3.8 THz and 6.2 THz. At this time, the absorption of about

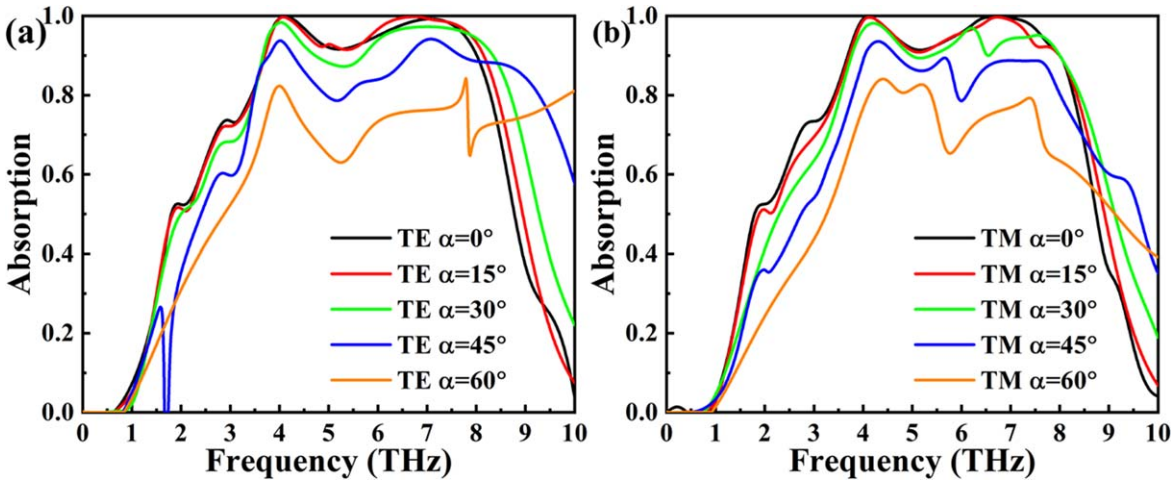

Figure 6. Absorption spectrum at different incident angles. (a) TE wave (b) TM wave.

Table 1. Different graphene broadband absorbers.

Absorber	Material	Absorption bandwidth	Tuning method
The absorber	Monolayer graphene	4.3 THz (3.7 THz–8 THz)	E_f and Physical parameters
Absorber 1[15]	Multilayer graphene	0.8 THz (3 THz–3.8 THz)	E_f and Physical parameters
Absorber 2 [16]	Dielectric materials and graphene	1.5 THz (1.6 THz–3.1 THz)	Untuned
Absorber 3 [23]	Alloy	3 THz (1.7 THz–4.7 THz)	Physical parameters
Absorber 4 [24]	Gold	0.8 THz (4.4 THz–5.2 THz)	Physical parameters
Absorber 5 [25]	Alloy	4.1 THz (7.9 THz–12 THz)	Physical parameters
Absorber 6 [35]	Monolayer graphene	2.5 THz (7 THz–9.5 THz)	E_f and Physical parameters

3.8 THz of the absorber is greater than 0.9 (3.6–7.4 THz). When E_f is 1.75 eV, the absorption peak of the absorber appears at 4.3 THz and 7.5 THz. At this time, the absorber has about 4.6 THz absorption greater than 0.9 (3.8–8.4 THz). When E_f is 2 eV, the absorption peak of the absorber appears at 4.3 THz and 7.5 THz. At this time, the absorber has about 4.6 THz absorption greater than 0.9 (4–8.6 THz). In conclusion, by changing E_f, absorption peaks λ_1 and λ_2 will move to different degrees, and the high absorption range and the intensity of the absorption peak of the absorber will change accordingly [47]. The shift range of absorption peak λ_1 is 3.7–4.3 THz, and the shift range of absorption peak λ_2 is 5.8–7.5 THz.

The high absorption range span of the absorber is between 0.9–4.6 THz. In the case mainly discussed in this paper ($E_f = 1.5$ eV), the absorption peaks λ_1 and λ_2 are perfect (higher than 0.99). The strong absorption range of the absorber is 4.3 THz (3.7–8 THz). It is obvious that the absorber has excellent tunability. Table 1 shows the comparison of the characteristics between different graphene broadband absorbers and the absorber proposed in this paper.

In order to enhance the practicability of the absorber, the influence of different electromagnetic wave incidence angles (α) on the absorber is investigated here, and the results are shown in figure 6. It is obvious that when the α increases from 0° to 30°, the absorbers show good stability (most of them maintain the absorptivity above 0.9 in 3.7–8THz). However, the absorption rate of the absorber mostly drops below 0.9 when the α is 45°. When the α is 60°, the absorptivity will be lower than 0.8. Due to the good polarization-independent property of the absorber, the absorption spectra of both mode waves at different α are basically the same.

4. Conclusion

This paper proposes a graphene-based terahertz bandwidth absorber. The absorber shows high absorption at 3.7–8 THz, and there are perfect absorption peaks at 4.1 THz and 6.7 THz. The absorber shows good polarization independence, and the relative impedance in the absorption region is approximate to that in free space. Through the analysis of the electric field diagram, the strong electric field coupling effect that brings about strong absorption is discussed, and by exploring the influence of physical parameters on the absorber, it is found that the absorber shows very high physical adjustability. Subsequently, the E_f was adjusted, and it was found that the absorber had good tunability. This means that the absorber will show excellent tunability by tuning the physical parameters and E_f. Finally, by studying the influence of different incident angles on the absorption spectrum, it is found that the absorber has a certain stability under different α. In general, the absorber can be used in medical research. Military science and technology, space exploration, and other

fields have huge application prospects and have a certain role in promoting the research of THz band bandwidth absorbers.

Acknowledgments

The authors are grateful for support from the National Natural Science Foundation of China (No. 51606158, 11604311, 12074151); funding from the Scientific Research Fund of Sichuan Provincial Science and Technology Department (2020YJ0137; 2020YFG0467; 2021JDRC0019); funding from the Opening Project of Key Laboratory of Microelectronic Devices & Integrated Technology, Institute of Microelectronics, Chinese Academy of Sciences; funding from the College Students' innovation and entrepreneurship training program (S202110619073; S202110619069); and funding from the undergraduate Innovation Fund Project of SWUST (CX 21-099; LX2020010; CX21-008).

Declaration of competing interest

The authors declare that they have no known competing financial interests or personal relationships that could have appeared to influence the work reported in this paper.

References

[1] Sizov F and Rogalski A 2010 THz detectors *Prog. Quantum Electron.* **34** 278–347
[2] Wu X L, Zheng Y, Luo Y, Zhang J G, Yi Z, Wu X W, Cheng S B, Yang W X, Yu Y and Wu P H 2021 A four-band and polarization-independent BDS-based tunable absorber with high refractive index sensitivity *Phys. Chem. Chem. Phys.* **23** 26864–73
[3] Sengupta K, Nagatsuma T and Mittleman D M 2018 Terahertz integrated electronic and hybrid electronic–photonic systems *Nat. Electron.* **1** 622–35
[4] Zheng Z P, Zheng Y, Luo Y, Yi Z, Zhang J G, Liu Z M, Yang W X, Yu Y, Wu X W and Wu P H 2022 Switchable terahertz device combining ultra-wideband absorption and ultra-wideband complete reflection *Phys. Chem. Chem. Phys.* **24** 2527–33
[5] Lee K, Choi H J, Son J, Park H S, Ahn J and Min B 2015 THz near-field spectral encoding imaging using a rainbow metasurface *Sci. Rep.* **5** 14403
[6] Chen H T, Padilla W J, Zide J M, Gossard A C, Taylor A J and Averitt R D 2006 Active terahertz metamaterial devices *Nature* **444** 597–600
[7] Zheng Z P, Luo Y, Yang H, Yi Z, Zhang J G, Song Q J, Yang W X, Liu C, Wu X W and Wu P H 2022 Thermal tuning of terahertz metamaterial properties based on phase change material vanadium dioxide *Phys. Chem. Chem. Phys.* **24** 8846–53
[8] Isozaki A, Kan T, Takahashi H, Matsumoto K and Shimoyama I 2015 Out-of-plane actuation with a sub-micron initial gap for reconfigurable terahertz micro-electro-mechanical systems metamaterials *Opt. Express* **23** 26243–51
[9] Wang D Y, Yi Z, Ma G L, Dai B, Yang J B, Zhang J F, Yu Y, Liu C, Wu X W and Bian Q 2022 Two channels photonic crystal fiber based on surface plasmon resonance for magnetic field and temperature dual-parameter sensing *Phys. Chem. Chem. Phys.* **24** 21233
[10] Nanni E A, Huang W R, Hong K H, Ravi K, Fallahi A, Moriena G, Miller R J and Kartner F X 2015 Terahertz-driven linear electron acceleration *Nat. Commun.* **6** 8486
[11] Liang S R, Xu F, Yang H, Cheng S B, Yang W X, Yi Z, Song Q J, Wu P H, Chen J and Tang C J 2023 Ultra long infrared metamaterial absorber with high absorption and broad band based on nano cross surrounding *Opt. Laser Technol.* **158** 108789
[12] Shangguan Q Y, Chen H, Yang H, Liang S R, Zhang Y J, Cheng S B, Yang W X, Yi Z, Luo Y and Wu P H 2022 A 'belfry-typed' narrow-band tunable perfect absorber based on graphene and the application potential research *Diam. Relat. Mater.* **125** 108973
[13] Chen H, Chen Z Z, Yang H, Wen L H, Yi Z, Zhou Z G, Dai B, Zhang J G, Wu X W and Wu P H 2022 Multi-mode surface plasmon resonance absorber based on dart-type single-layer graphene *RSC Adv.* **12** 7821–9
[14] Cheng T T, Gao H J, Liu G R, Pu Z S, Wang S F, Yi Z, Wu X W and Yang H 2022 Preparation of core–shell heterojunction photocatalysts by coating CdS nanoparticles onto $Bi4Ti_3O_{12}$ hierarchical microspheres and their photocatalytic removal of organic pollutants and Cr(VI) ions *Colloids Surf. A: Physicochem. Eng. Asp.* **633** 127918
[15] Wang Y, Song M, Pu M, Gu Y, Hu C, Zhao Z, Wang C, Yu H and Luo X 2016 Staked graphene for tunable terahertz absorber with customized bandwidth *Plasmonics* **11** 1201–6
[16] Yang J, Zhu Z, Zhang J, Guo C, Xu W, Liu K, Yuan X and Qin S 2018 Broadband terahertz absorber based on multi-band continuous plasmon resonances in geometrically gradient dielectric-loaded graphene plasmon structure *Sci. Rep.* **8** 3239
[17] Tao H, Landy N I, Bingham C M, Zhang X, Averitt R D and Padilla W J 2008 A metamaterial absorber for the terahertz regime: design, fabrication and characterization *Opt. Express* **16** 7181–8
[18] Landy N I, Sajuyigbe S, Mock J J, Smith D R and Padilla W J 2008 Perfect metamaterial absorber *Phys. Rev. Lett.* **100** 207402
[19] Adomanis B M *et al* 2015 Bi-layer metamaterials as fully functional near-perfect infrared absorbers *Appl. Phys. Lett.* **107** 021107
[20] Shangguan Q Y, Zhao Y, Song Z J, Wang J, Yang H, Chen J, Liu C, Cheng S B, Yang W X and Yi Z 2022 High sensitivity active adjustable graphene absorber for refractive index sensing applications *Diam. Relat. Mater.* **128** 109273
[21] Lin X, Li M, Li Y J and Chen, W 2015 Enhancement of the catalytic activity of ordered mesoporous TiO_2 by using carbon fiber support and appropriate evaluation of synergy between surface adsorption and photocatalysis by Langmuir-Hinshelwood (L-H) integration equation *RSC Adv.* **5** 105227–38
[22] Wang X Y, Lin J C, Yan Z Y, Yi Z, Yu J X, Zhang W, Qin F, Wu X W, Zhang J G and Wu P H 2022 Tunable high-sensitivity sensing detector based Bulk Dirac semimetal *RSC Adv.* **12** 32583
[23] Wang B X, Wang L L, Wang G Z, Huang W Q, Li X F and Zhai X 2014 A simple design of a broadband, polarization-insensitive, and low-conductivity alloy metamaterial absorber *Appl. Phys. Express* **7** 082601
[24] Wen Y, Ma W, Bailey J, Matmon G and Yu X 2015 Broadband terahertz metamaterial absorber based on asymmetric resonators with perfect absorption *IEEE Trans. Terahertz Sci. Technol.* **5** 406–11
[25] Guo W, Liu Y and Han T 2016 Ultra-broadband infrared metasurface absorber *Opt. Express* **24** 20586–92

[26] Cai L, Zhang Z H, Xiao H M, Chen S and Fu J L 2019 An eco-friendly imprinted polymer based on graphene quantum dots for fluorescent detection of p-nitroaniline *RSC Adv.* **9** 41383–91
[27] Long F, Zhang Z H, Wang J, Yan L, Lu P P and Yang Z X 2016 Magnetic graphene modified imprinted electrochemical sensor for detection of 4-Octylphenol *Chin. J. Anal. Chem.* **44** 908–14
[28] Long F, Zhang Z H, Wang J, Yan L and Zhou B W 2015 Cobalt-nickel bimetallic nanoparticles decorated graphene sensitized imprinted electrochemical sensor for determination of octylphenol *Electrochim. Acta* **168** 337–45
[29] Zhang Z H, Cai R, Long F and Wang J 2015 Development and application of tetrabromobisphenol a imprinted electrochemical sensor based on graphene/carbon nanotubes three-dimensional nanocomposites modified carbon electrode *Talanta* **134** 435–42
[30] Lin X, Li Y J, Chen F T, Xu P and Li M 2017 Facile synthesis of mesoporous titanium dioxide doped by Ag-coated graphene with enhanced visible-light photocatalytic performance for methylene blue degradation *RSC Adv.* **7** 25314–24
[31] Shangguan Q Y, Chen Z H, Yang H, Cheng S B, Yang W X, Yi Z, Wu X W, Wang S F, Yi Y G and Wu P H 2022 Design of ultra-narrow band graphene refractive index sensor *Sensors* **22** 6483
[32] Chen C L, Wang Y, Yi Z, Wang S F, Ma J Y, Gao H J, Wu X W, Liu G R and Yang H 2022 PH-induced structural evolution, photodegradation mechanism and application of bismuth molybdate photocatalyst *Adv. Powder Technol.* **33** 103858
[33] Wang B X, Zhai X, Wang G Z, Huang W Q and Wang L L 2015 Design of a four-band and polarization-insensitive terahertz metamaterial absorber *IEEE Photonics J.* **7** 1–8
[34] Xiong H, Wu Y B, Dong J, Tang M C, Jiang Y N and Zeng X P 2018 Ultra-thin and broadband tunable metamaterial graphene absorber *Opt. Express* **26** 1681–8
[35] Liu C, Qi L and Zhang X 2018 Broadband graphene-based metamaterial absorbers *AIP Adv.* **8** 015301
[36] Zhou F Q, Qin F, Yi Z, Yao W T, Liu Z M, Wu X W and Wu P H 2021 Ultra-wideband and wide-angle perfect solar energy absorber based on Ti nanorings surface plasmon resonance *Phys. Chem. Chem. Phys.* **23** 17041–8
[37] Deng Y, Cao G T, Yang H, Zhou X Q and Wu Y W 2018 Dynamic control of double plasmon-induced transparencies in aperture-coupled waveguide-cavity system *Plasmonics* **13** 345–52
[38] Deng Y, Cao G, Wu Y, Zhou X and Liao W 2015 Theoretical description of dynamic transmission characteristics in MDM waveguide aperture-side-coupled with ring cavity *Plasmonics* **10** 1537–43
[39] Zhang J, Zhu Z, Liu W, Yuan X and Qin S 2015 Towards photodetection with high efficiency and tunable spectral selectivity: graphene plasmonics for light trapping and absorption engineering *Nanoscale* **7** 13530–6
[40] Chen J, Chen S Y, Gu P, Yan Z D, Tang C J, Xu Z J, Liu B and Liu Z Q 2020 Electrically modulating and switching infrared absorption of monolayer graphene in metamaterials *Carbon* **162** 187–94
[41] Zhao F, Lin J C, Lei Z H, Yi Z, Qin F, Zhang J G, liu L, Wu X W, Yang W X and Wu P H 2022 Realization of 18.97% theoretical efficiency of 0.9 μm Thick c-Si/ZnO heterojunction ultrathin-film solar cells via surface plasmon resonance enhancement *Phys. Chem. Chem. Phys.* **24** 4871–80
[42] Liu Y H, Bo M L, Yang X X, Zhang P P, Sun C Q and Huang Y L 2017 Size modulation electronic and optical properties of phosphorene nanoribbons: DFT-BOLS approximation *Phys. Chem. Chem. Phys.* **19** 5304–9
[43] Zhang C, Yi Y T, Yang H, Yi Z, Chen X F, Zhou Z G, Yi Y G, Li H L, Chen J and Liu C 2022 Wide spectrum solar energy absorption based on germanium plated ZnO nanorod arrays: energy band regulation, finite element simulation, super hydrophilicity, photothermal conversion *Appl. Mater. Today* **28** 101531
[44] Li L X, Gao H J, Yi Z, Wang S F, Wu X W, Li R S and Yang H 2022 Comparative investigation on synthesis, morphological tailoring and photocatalytic activities of $Bi_2O_2CO_3$ nanostructures *Colloids Surf. A: Physicochem. Eng. Asp.* **644** 128758
[45] Cao G, Li H, Deng Y, Zhan S, He Z and Li B 2014 Systematic theoretical analysis of selective-mode plasmonic filter based on aperture-side-coupled slot cavity *Plasmonics* **9** 1163–9
[46] Gu Y F, Guo B B, Yi Z, Wu X W, Zhang J and Yang H 2022 Synthesis of a self-assembled dual morphologies Ag-NPs/$SrMoO_4$ photocatalyst with LSPR Effect for the degradation of methylene blue dye *ChemistrySelect* **7** e202201274
[47] Zhu X Z, Cheng Y Z, Fan J P, Chen F, Luo H and Wu L 2022 Switchable efficiency terahertz anomalous refraction and focusing based on graphene metasurface *Diam. Relat. Mater.* **121** 108743